

Porous Carbons Derived from Lignite Mixed with Zn²⁺-Doped Lignin for Electric Double-Layer Capacitor

Yan Wu, Xiao-Yan Zhao*, Jing-Pei Cao**, Shan He, Zhi-Qiang Hao, Hua-Yang Yu, Guo-Yu Sun, Xian-Yong Wei

Key Laboratory of Coal Processing and Efficient Utilization (Ministry of Education), China University of Mining & Technology, Xuzhou 221116, Jiangsu, China

*E-mail: zhaoxiaoyan@cumt.edu.cn

**E-mail: caojingpei@cumt.edu.cn, beyondcao@hotmail.com, beyondcao_2000@163.com

Received: 3 June 2017 / Accepted: 11 July 2017 / Published: 13 August 2017

A series of porous carbons (PCs) were prepared from lignin chelating with Zn²⁺ and mixed with lignite. KOH was used as the activated agent during preparation process. The influences of preparation parameters including the content of lignin chelated with Zn²⁺, KOH/sample ratio and activation temperature on specific surface area (SSA), pore size distribution and electrochemical performances were investigated in this study. All the PCs were mainly micropores through nitrogen adsorption isotherms test. The PCs derived from the lignin chelating with Zn²⁺ present high SSA and total pore volume than that in the absence of Zn²⁺. In addition, the PC prepared from adding lignin to lignite has larger SSA than the PC prepared from lignite. The PC prepared with Zn²⁺ account for 30% of lignin mass, KOH/sample ratio of 3:1 and activation temperature of 700 °C has the largest SSA of 3311 m² g⁻¹. When it was used as electrode for electric double-layer capacitor, the specific capacitance reached the highest value of 280.43 F g⁻¹ at a current density of 40 mA g⁻¹. The results demonstrate that the lignin chelating with Zn²⁺ then add to the lignite can significantly improve PCs performance.

Keywords: Lignin; Lignite; Porous carbons; High surface area; EDLC

1. INTRODUCTION

The electric motors and generators invented in 1870s lead to a prevalence of the electrical energy, especially in the age of electricity [1]. Nowadays, the oil resources scarcity and the environment problems are becoming more and more serious which are pushing people to find an environmentally effective energy storage device [2]. The supercapacitor as a promising energy storage

devices for electric power have been attracting much attention [3], which ascribed to its high energy density, long cycle life and excellent reversibility [4, 5]. The supercapacitor can be divided into electric double-layer capacitor (EDLC), pseudocapacitive and hybrid capacitors according to its storage mechanism [2, 3, 6].

In general, the electrode materials is the core component to EDLC. The electrode materials with high specific surface area (SSA), optimized porous structures and favorite functional groups has excellent electrochemical performance. A series of porous carbons (PCs) such as activated carbons, carbon nanotubes, carbon aerogels, graphene sheets and carbon nanofibers [7-11] were used for EDLC. The PCs can be prepared from waste tea-leaves, sugar cane bagasse, coal, pitch and petroleum coke [12-17]. The preparation methods of PCs include physical and chemical activation, among which chemical activation is known as a simple method for preparation of PCs with high SSA and porosity.

Lignin is the second most abundant natural polymer next to cellulose and can be used as a precursor for PCs attribute to its most abundant aromatic polymer [18-20]. Hong et al. [21] reported that the $ZnCl_2$ can act not only as solvent for lignin, but also can integrated into the lignin. The metal ion has the capability of promoting the dehydrogenation of the polymer and catalyzing char formation in the condensed phase [22]. Coal are usually as the precursors for preparation of PCs due to the low cost and high carbon content, especially for that rich in oxygen functional group, such as lignite. But the high ash content in lignite has a great impact on the quality of PCs. When PCs was used as electrode materials for EDLC, the ash also affect the EDLC performances [23]. Addition of certain carbonaceous materials to the lignite may improve the performance of PCs. KOH is one of the most effective compound for preparation of activated carbons. The PCs prepared from the mixture (lignin treated by $ZnCl_2$ then add to the lignite) which may be have a high SSA when KOH was used as activating agent. The PCs prepared through this method and applied in EDLC may have excellent electrochemical performance, which are rarely reported.

In this work, the lignin was firstly mixed with $ZnCl_2$ solution to obtain the lignin with Zn^{2+} . Then the PCs were prepared from the mixture which the lignin with Zn^{2+} add to lignite through carbonization-activation method. The effects of Zn^{2+} content, KOH/sample ratio and activation temperatures on the SSA and electrochemical performance of the PCs for EDLC in 6 M KOH electrolyte were addressed in detail.

2. EXPERIMENTAL

2.1. Materials and Reagents

Alkali lignin was purchased from TCI and Shengli lignite was collected from Inner Mongolia, China. The proximate and ultimate analyses of lignin and lignite were shown in Table 1. $ZnCl_2$ and KOH are both the analytical reagents provided by Xilong Chemical Co. Deionized water was used through all the experiment.

Table 1. Proximate and ultimate analyses of the lignin and lignite.

Sample	Proximate analysis (wt%)				Ultimate analysis (wt%,daf)				
	M _{ar}	A _d	VM _d	FC _d ^a	C	H	N	S	O ^a
Lignin	4.0	16.8	48.7	34.5	64.9	7.3	0.3	7.7	19.8
Lignite	12.8	18.7	43.6	37.7	67.5	4.9	1.3	0.5	25.8

A: ash; M: moisture; VM: volatile matter; FC: fixed carbon; ar: as received basis; d: dried basis; daf: dried and ash free basis; a: by difference.

2.2. Preparation of the PCs

Lignin was added to the ZnCl₂ solution and the content of Zn²⁺ was calculated based on the weight of the lignin. The lignin and ZnCl₂ solution were stirred for 1 h in the water bath at 60 °C, and then dried at 105 °C for 24 h. Subsequently, the lignin with Zn²⁺ was mixed with lignite (the weight ratio was 1:1). The mixture was carbonized at 600 °C for 2 h under Ar atmosphere in a horizontal tube furnace at a heating rate of 10 °C min⁻¹. And the obtained char was denoted as LC. The LC was activated with KOH in a horizontal tube furnace at 180 °C for 30 min and then at prescribed temperature of 600 to 900 °C for 1 h. The activated samples were boiled at 80 °C with 2 M HCl solution for 30 min, filtered and rinsed by warm deionized water several times, and then washed by room-temperature deionized water until neutral. The washed sample was dried in a vacuum oven at 150 °C for 3 h and the sample was denoted as PC. All the samples and their preparation parameters in this study are shown in Table 2. The lignite without lignin is named SL and the lignin without lignite is named LG. The preparation condition of SL and LG is the same to PC-7.

Table 2. The preparation parameters of PCs (carbonization temperature of 600 °C and activation time of 60 min).

Sample	Ratio (KOH:LC)	Content of zinc ions (%)	Activation temperature (°C)
PC-1	3:1	-	700
PC-2	3:1	10	700
PC-3	3:1	30	700
PC-4	3:1	50	700
PC-5	1:1	30	700
PC-6	2:1	30	700
PC-7	4:1	30	700
PC-8	5:1	30	700
PC-9	3:1	30	600
PC-10	3:1	30	800
PC-11	3:1	30	900

2.3. Carbon Characterization

Nitrogen adsorption-desorption isotherms were measured at 77 K using an automatic adsorption system in a Quantachrome Autosorb-IQ automated gas sorption analyzer. In order to

eliminate surface contamination, all the samples were degassed at 300 °C for 10 h in a vacuum condition before adsorption. The SSA and pore size distributions were calculated by using the Brunauer-Emmett-Teller (BET) equation and the Density Functional Theory (DFT), respectively. The total pore volume (V_t) was estimated at a relative pressure of P/P_0 of 0.99. In addition, the micropore surfaces and micropore volumes were measured using the t-plot method. The macroscopic features of samples were obtained on a Merlin Zeiss scanning electron microstructure (SEM).

2.4. Electrochemical Measurements

The electrodes were prepared by mixing PC, acetylene black and polytetrafluoroethylene (PTFE) binder at a weight ratio of 85:10:5 in an agate mortar and then the mixture was pressed onto nickel foam under 6 MPa in wafer shape with a diameter of 13 mm. The electrodes were immersed with 6 M KOH solution under vacuum for 24 h to guarantee thorough wetting. Two of the electrodes were assembled at room temperature and separated by polypropylene membrane, using MTI EQ-STC two-electrode testing type system. Cyclic voltammetry (CV) and electrochemical impedance spectroscopy (EIS) were carried out on an Ivium Vertex electrochemical workstation. CV was performed at a voltage ranging from 0 to 1 V at different scan rates. EIS measurement was measured at the open circuit voltage with amplitude of 10 mV and the frequency range from 10^{-2} to 10^5 Hz. Galvanostatic charge-discharge (GCD) was tested with the voltage from 0 to 0.9 V by NEWARE cell test instrument. The specific capacitance (C_s) was calculated from the galvanostatic discharge curves according to Eq. (1) [24].

$$C_s = 2 \frac{I\Delta t}{m\Delta V} \quad (1)$$

Where C_s is the specific capacitance ($F\ g^{-1}$), I is the current of discharge, Δt is the discharge time, m is one of the mass of electrodes material and ΔV is the voltage difference.

The energy density ($W\ h\ kg^{-1}$) and power density ($W\ kg^{-1}$) were calculated based on the following formula [25]:

$$E = \frac{1}{2} CV^2 \quad (2)$$

$$P = \frac{VI}{m} \quad (3)$$

Where I is the discharge current and m is the active mass of the two-electrode capacitor.

3. RESULTS AND DISCUSSION

3.1. Structural Characterization of the PCs

3.1.1. Morphology and Microstructure of the PCs

As shown in Fig. 1a, a large number of Zn^{2+} can be found with uneven distribution that due to the uneven lignin mixed with lignite. It also suggests that the Zn^{2+} are successfully introduced into the precursor mixture. The image of Fig. 1b displays an uneven surface with many small pores and no zinc

elements residual can be observed. ZnCl_2 evaporates and leave the position previously occupied by ZnCl_2 during the activation process. The result is that the PCs present high SSA, which is also supported by the nitrogen adsorption-desorption isotherms. The PC-1 (Fig. 1c) has porous structure with rugged surface structure. Compared with PC-3, the PC-1 has few pores demonstrating that the mixture of lignite and lignin chelating with Zn^{2+} during the activation process can make more pores than that in the absence of Zn^{2+} .

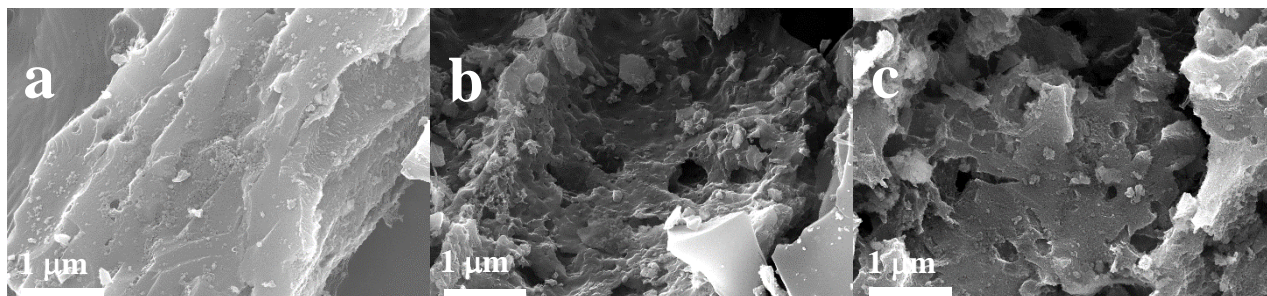


Figure 1. SEM images of the LC contain 30% zinc ions (a); PC-3 (b); PC-1 (c).

3.1.2. Pore Structure of PCs

It is well known that the pore size distribution and SSA are the important parameters for EDLC. The perfect carbon electrodes need proper pore size distribution and relatively high SSA [26]. Thus it is necessary to study the pore structure of prepared PCs and understand the effects of preparation conditions on the development of pore structure. Nitrogen adsorption-desorption analysis were carried out to study the porosity of PCs.

As exhibited in Fig. 2, the PCs are typical of microporous materials and nitrogen adsorption-desorption isotherms are belong to type I according to the classification of the IUPAC [27]. The nitrogen adsorption sharply increases at relative pressure below 0.4, which illustrates a large number of micropores in the PCs. A hysteresis loop can be found at the P/P_0 of 0.4-0.9, which reveals the presence of mesopores in PCs. In addition, small tails at the P/P_0 near 1.0 revealing the presence of macropores. The SSA, pore volume and average pore size parameters of the PCs are given in Table 3.

As shown in Fig. 2a, the isotherms rises rapidly at low relative pressure with the increase of the Zn^{2+} amount, indicating that the Zn^{2+} plays an important role in microporous producing. It should be attributed to the dehydration of ZnCl_2 during the activation process, which results in the carbonization and aromatization of carbon skeleton and pore-creating [24]. Some researchers are using ZnCl_2 as activated agent for production of activated carbons [2, 28-30]. The adsorption quantity increased from PC-1 to PC-3, while the adsorption capacity decreased with the increase of Zn^{2+} content from 30% to 50%. It probably due to the excess Zn^{2+} cause some pores become larger even collapse during activation process and leading to a reduction of SSA.

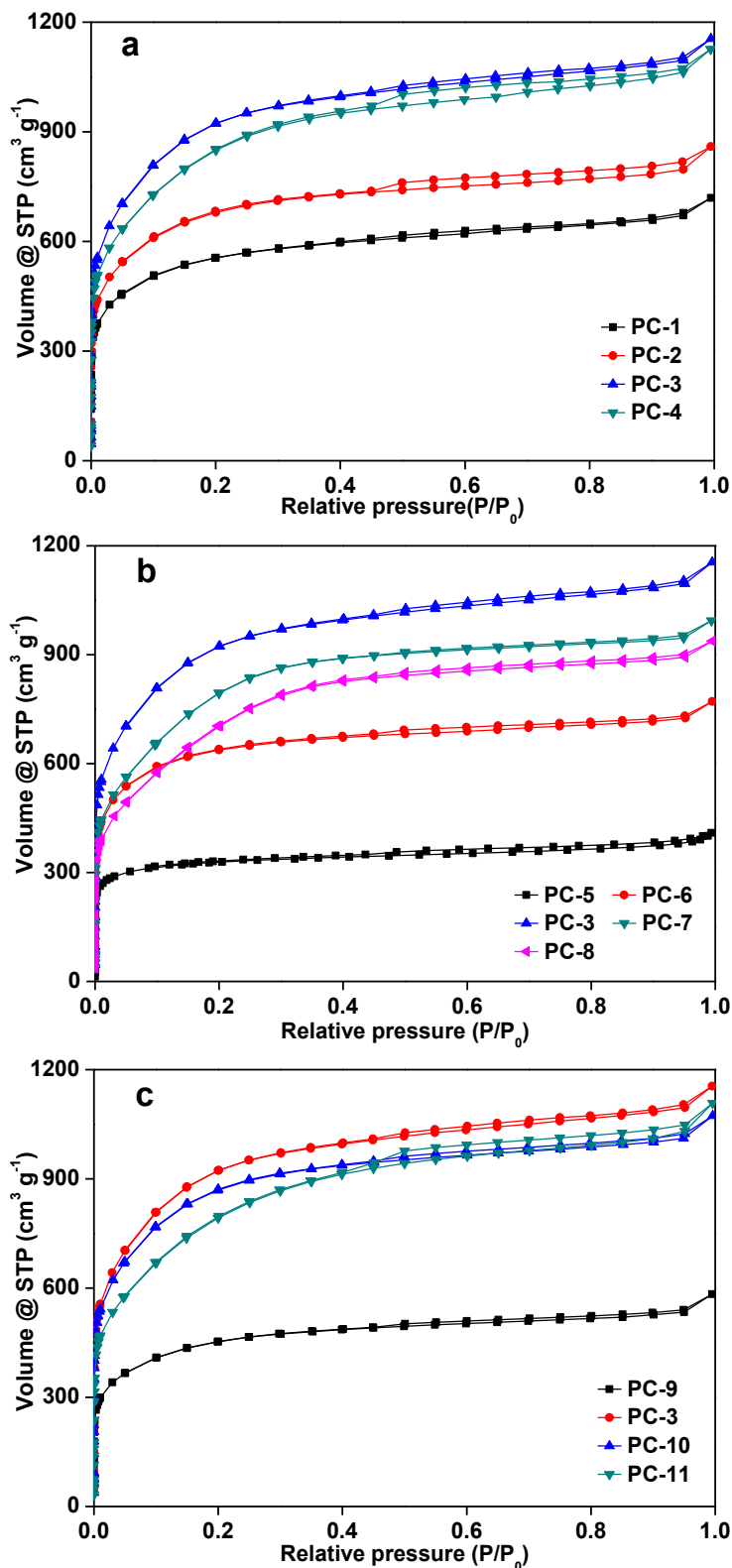


Figure 2. Nitrogen adsorption-desorption isotherms of the PCs.

The KOH-LC ratio also has a significant influence on the pore structure [14]. As listed in Table 3, with KOH-LC ratio from 1:1 to 5:1, the SSA is 1257, 2351, 3311, 2842 and 2518 $\text{m}^2 \text{g}^{-1}$, and the V_t is 0.63, 1.19, 1.79, 1.54 and 1.45 $\text{cm}^3 \text{g}^{-1}$, respectively. The trend of SSA and V_t is increased firstly and

then decreased with the increase of KOH-LC ratio. The trend indicated that the activation by KOH could make micropores etched into mesopores or macropores. However, the excessive amounts of KOH could leads to pores collapse and resulting in the reduction of SSA [31, 32]. It also can be seen that the PC-7 has higher SSA than SL and LG, indicating that lignin chelating with Zn^{2+} then add to lignite can improve the quality of PCs. The lignin pyrolysis is wider than lignite (Fig. 3a and b). The lignin may be release of CO_2 and CO and form some pores at low temperature. With the activation process continues, more CO_2 and CO are released from the mixture and developed more pores. The results is that the PC-7 has large SSA ($2842 \text{ m}^2 \text{ g}^{-1}$). Li et al. [33] prepared activated carbon from lignite with $ZnCl_2$ and the SSA of the as prepared activated carbon was only $1024 \text{ m}^2 \text{ g}^{-1}$.

Table 3. Pore structure parameters of the PCs obtained under different preparation conditions.

Sample	S_{BET}^a ($\text{m}^2 \text{ g}^{-1}$)	S_{micro}^b ($\text{m}^2 \text{ g}^{-1}$)	$S_{non-micro}^c$ ($\text{m}^2 \text{ g}^{-1}$)	V_{tot}^d ($\text{cm}^3 \text{ g}^{-1}$)	V_{micro}^b ($\text{cm}^3 \text{ g}^{-1}$)	$V_{non-micro}^c$ ($\text{cm}^3 \text{ g}^{-1}$)	D^e (nm)
PC-1	2015	1790	225	1.11	0.80	0.31	2.21
PC-2	2451	2242	209	1.33	1.01	0.32	2.17
PC-3	3311	2953	358	1.79	1.34	0.45	2.16
PC-4	3016	2674	342	1.74	1.28	0.46	2.31
PC-5	1257	1150	107	0.63	0.47	0.16	2.01
PC-6	2351	2197	154	1.19	0.95	0.24	2.03
PC-7	2842	2652	190	1.54	1.27	0.27	2.16
PC-8	2518	2294	224	1.45	1.16	0.29	2.30
PC-9	1634	1467	167	0.90	0.66	0.24	2.21
PC-10	3121	2871	250	1.66	1.31	0.35	2.13
PC-11	2814	2431	283	1.71	1.21	0.50	2.44
SL	2675	2490	185	1.35	1.14	0.21	2.02
LG	2295	2155	140	1.04	0.91	0.13	1.81

^a S_{BET} : Specific surface area from multiple BET method.

^b S_{micro} , V_{micro} : Micropore surface area micropore volume from t-plot method.

^c $S_{non-micro}$, $V_{non-micro}$: Difference of S_{BET} and S_{micro} and total pore volume and V_{micro} , respectively.

^d V_{tot} : Total pore volume at $P/P_0 = 0.99$.

^e D: Average pore diameter.

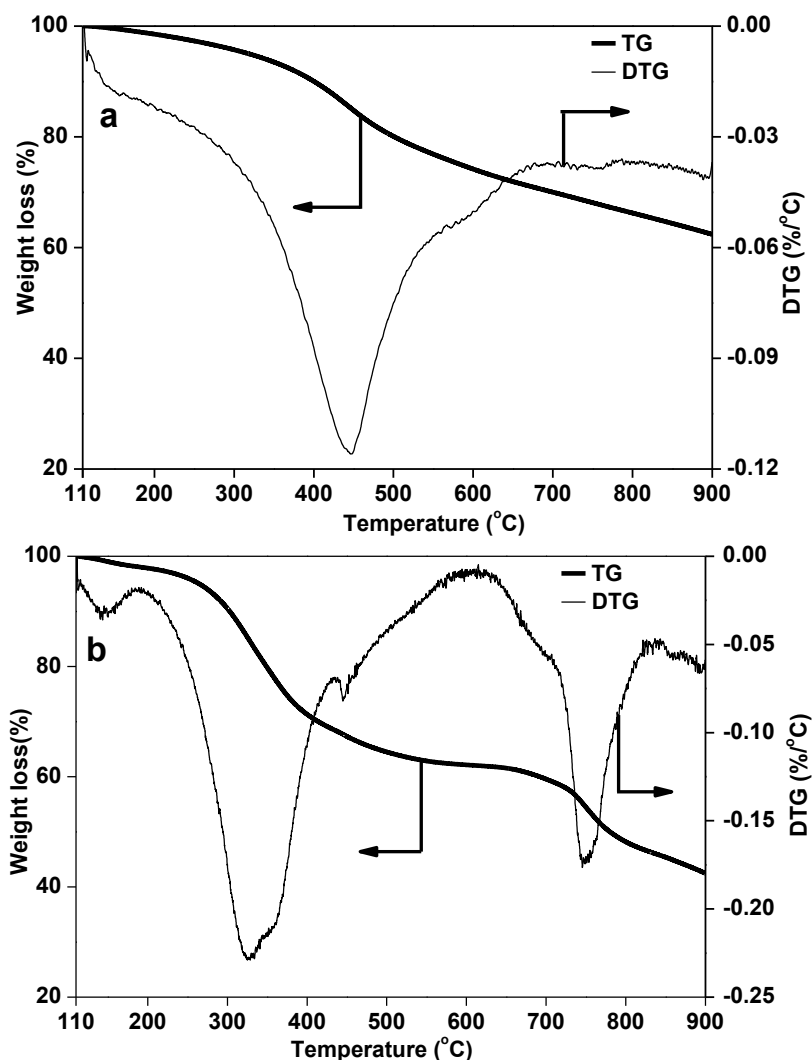


Figure 3. TG and DTG curves of lignite (a) and lignin (b).

Activation temperature is also an important factor for controlling activation extent [34]. The increase of activation temperature from 600 °C to 700 °C caused the increase of both the SSA and mesopores size. However, the SSA decreased from 3311 to 2814 m² g⁻¹ when the activation temperature was increased from 700 °C to 900 °C, which is ascribed to the fact that the activation reaction over 700 °C is fast and thus results in over-etching [32, 35].

As can be deduced from Fig. 4, the pore diameters of all the PCs concentrate in a range of 0.5 to 5 nm, illustrating that the PCs mainly contained micropores and mesopores, which is consistent with the nitrogen adsorption-desorption isotherms. Some researchers reported that micropores and mesopores with pore width in a certain rang is favor for charge storage in aqueous electrolytes [36-38].

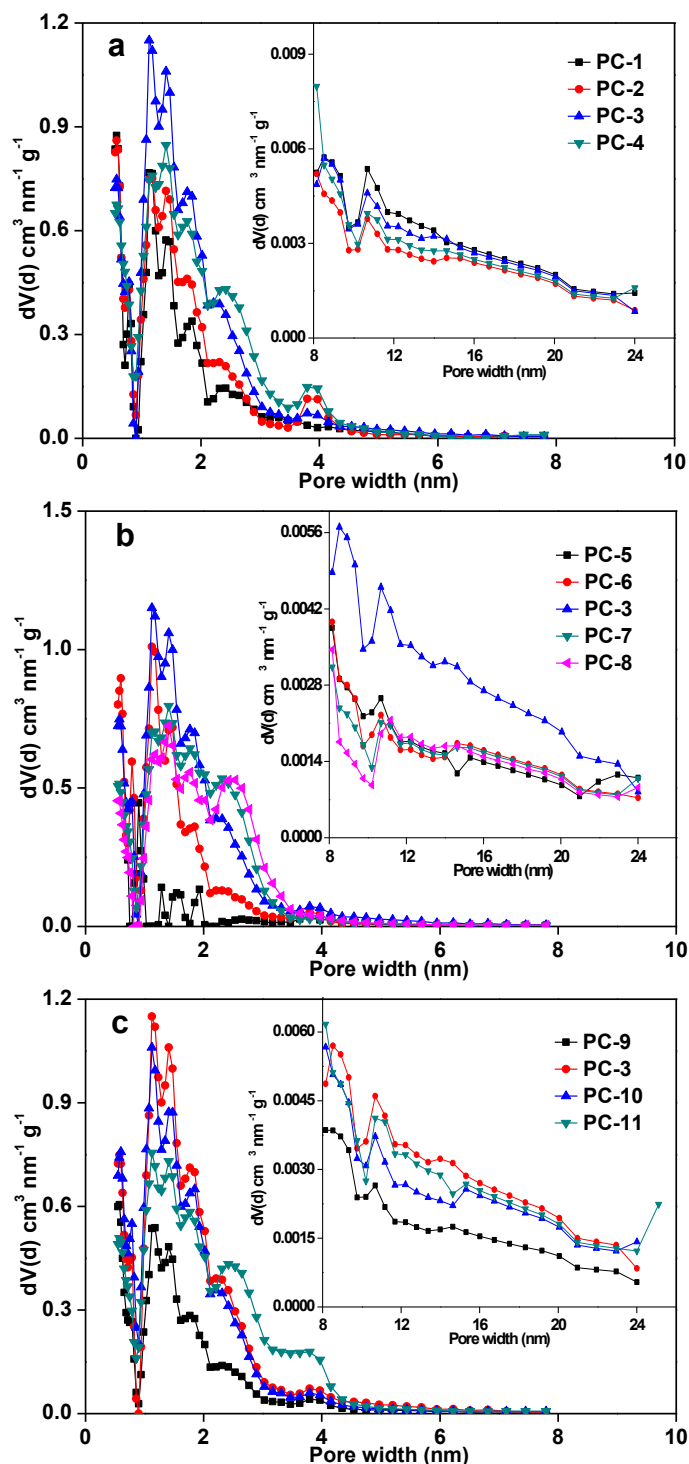


Figure 4. Pore size distributions of the PCs.

3.2. The Influence of Preparation Conditions on the Electrochemical Properties

3.2.1. Effect of Zn^{2+} Content

The GCD measurements were used to detect the electrochemical performances of the obtained PCs. As can be seen from Fig. 5a, the curves of the PCs present closely linear and symmetrical triangle

with low iR voltage drops which indicate the good electrochemical reversibility of the PCs [39]. The charge-discharge time of PC-3 is much longer than the others, suggesting the PC-3 has higher C_s (280.43 F g^{-1}). The good performance of PC-3 should be attributed to the highest SSA (Table 3). The C_s can be calculated according to the Eq. (1). The C_s values at the current density of 40 mA g^{-1} are 198.94, 241.92, 280.43 and 261.11 F g^{-1} for the PC-1, PC-2, PC-3 and PC-4, respectively, demonstrating that the PC-3 is the most appropriate for energy storage.

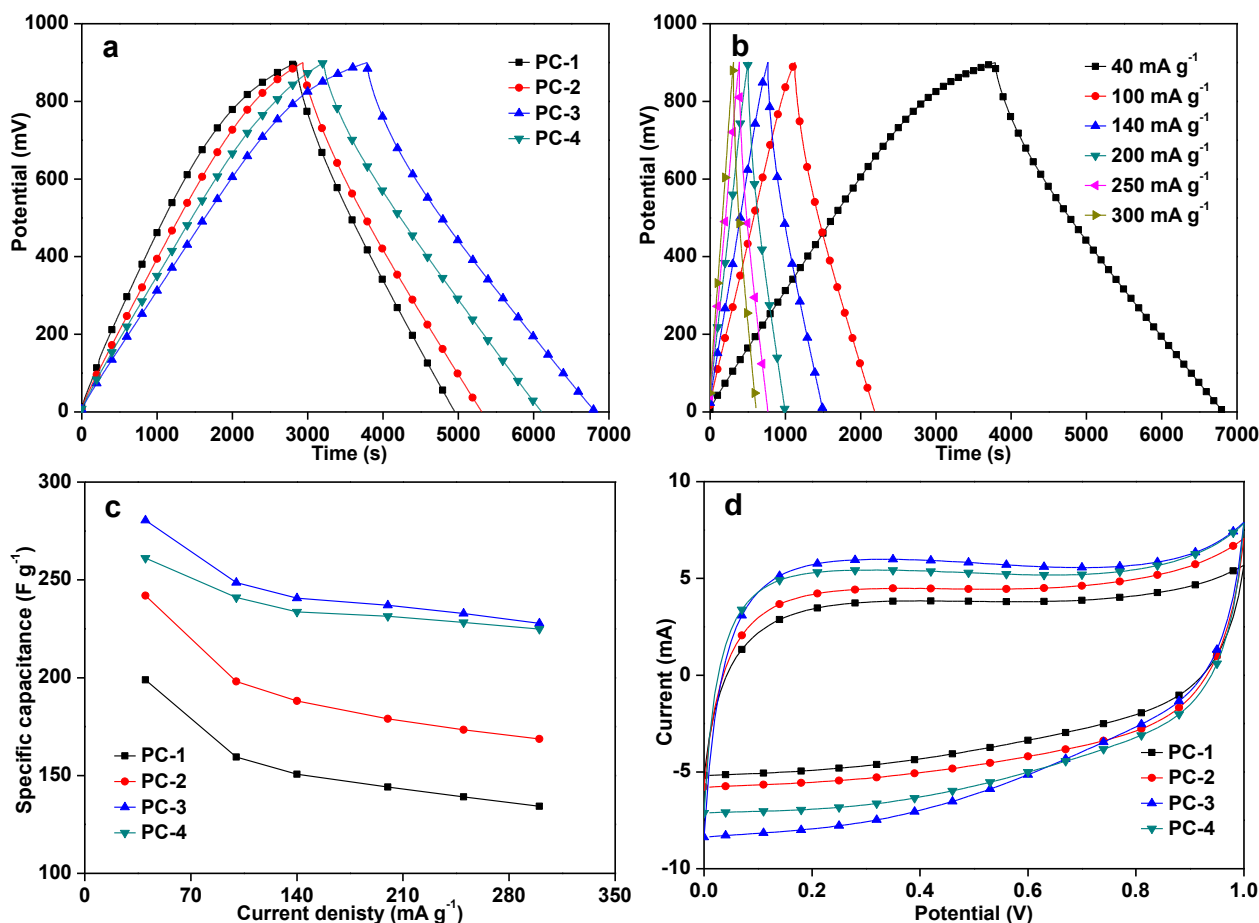


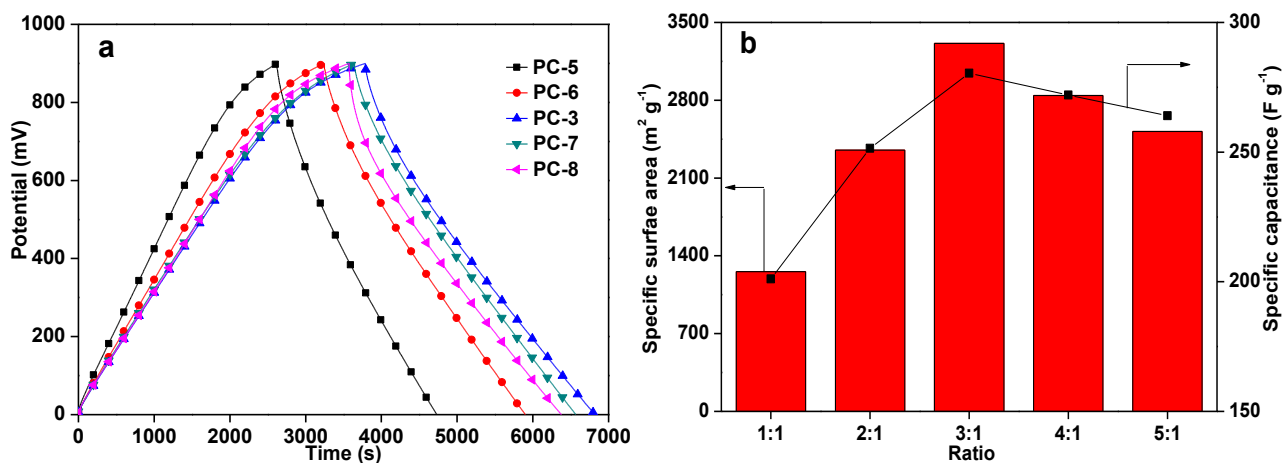
Figure 5. Effect of Zn^{2+} content on the capacitive performances of PCs (PC-1~ PC-4). GCD curves of PCs at 40 mA g^{-1} (a); GCD curves of PC-3 at different current densities (b); C_s of PCs at different current densities (c); CV curves of PCs at a scan rate of 2 mV s^{-1} (d).

Fig. 5b displays the GCD curves of PC-3 at different current densities. All the curves are still approximate isosceles triangle at increased current densities from 40 to 300 mA g^{-1} , suggesting excellent electrochemical reversibility [40]. The relationship between the current density and C_s is given in Fig. 5c. The C_s decreases with the increasing of current density, which is due to the slow charge-discharge kinetics of the electrode material. Therefore, at the relatively high current density, the electrolyte ions has not enough time to access the surface of carbon so that a large number of ions was not been well used [2]. The other one is that the electrolyte ions diffusion in the porous suffered great resistance and the ions cannot fully enter the micropores under high current density [41].

CV can be further illustrate the electrochemical performance of the PCs. As seen in Fig. 5d, the CV curves show a typical similar rectangular shape without clear redox peaks indicating an ideal EDLC behavior and a fast diffusion of electrolyte ions into/out of the electrode materials [42]. In addition, the CV curve of PC-3 has larger area than that of PC-1, PC-2 and PC-4. In general, a large SSA will have a high C_s . The relatively high C_s of PC-3 is consistent with the result of GCD curves in Fig. 5a.

3.2.2. The Effect of KOH-LC Ratio

As exhibits in Table 3, the SSA and V_t were changed with the increase of KOH-LC ratio which leading to the electrochemical properties change. Fig. 6a shows the approximate isosceles triangle shape of the PC-5, PC-6, PC-3, PC-7 and PC-8 curves, indicating that the samples have good electrochemical stability and reversibility. The C_s at the current density of 40 mA g^{-1} of the PC-5, PC-6, PC-3, PC-7 and PC-8 is 201.10 , 251.42 , 280.43 , 271.98 and 264.03 F g^{-1} , respectively. The relatively high C_s of PC-3 (KOH/LC = 3) is consistent with the high SSA and pore volume. As shown in Fig. 6b, the SSA increased rapidly with the increase of KOH-LC ratio from 1 to 3 and reached $3311 \text{ m}^2 \text{ g}^{-1}$ when the KOH/LC is 3. The SSA decreased when further increased the ratio above 3. The change in C_s is similar to the SSA, suggesting the SSA has important influences on the C_s . The result is consistent with that reported by Gamby [43]. It can be seen in Fig. 6c that all the CV curves display a similar rectangles shape without redox peaks, indicating the typical performance of EDLC. Fig. 6d shows the CV curves of PC-3 at different scan rates from 2 to 100 mV s^{-1} . The shapes of the CV curves deviate from the rectangular and became more and more oblique with the increase of scan rate. It because that the increase of scan rate caused the voltage signal could not reach the pores effectively. In other words, this phenomenon should be attributed to the tardiness of the charge-discharge kinetics of the PC. Therefore, the electrolyte ions cannot reach the PC surface efficiently in a short time [44, 45]. Compared with SL and LG, the PC-7 has larger C_s (Fig. 6e) which due to the PC-7 has large SSA. The results illustrate that the electrochemical performance improve after adding lignin to lignite.



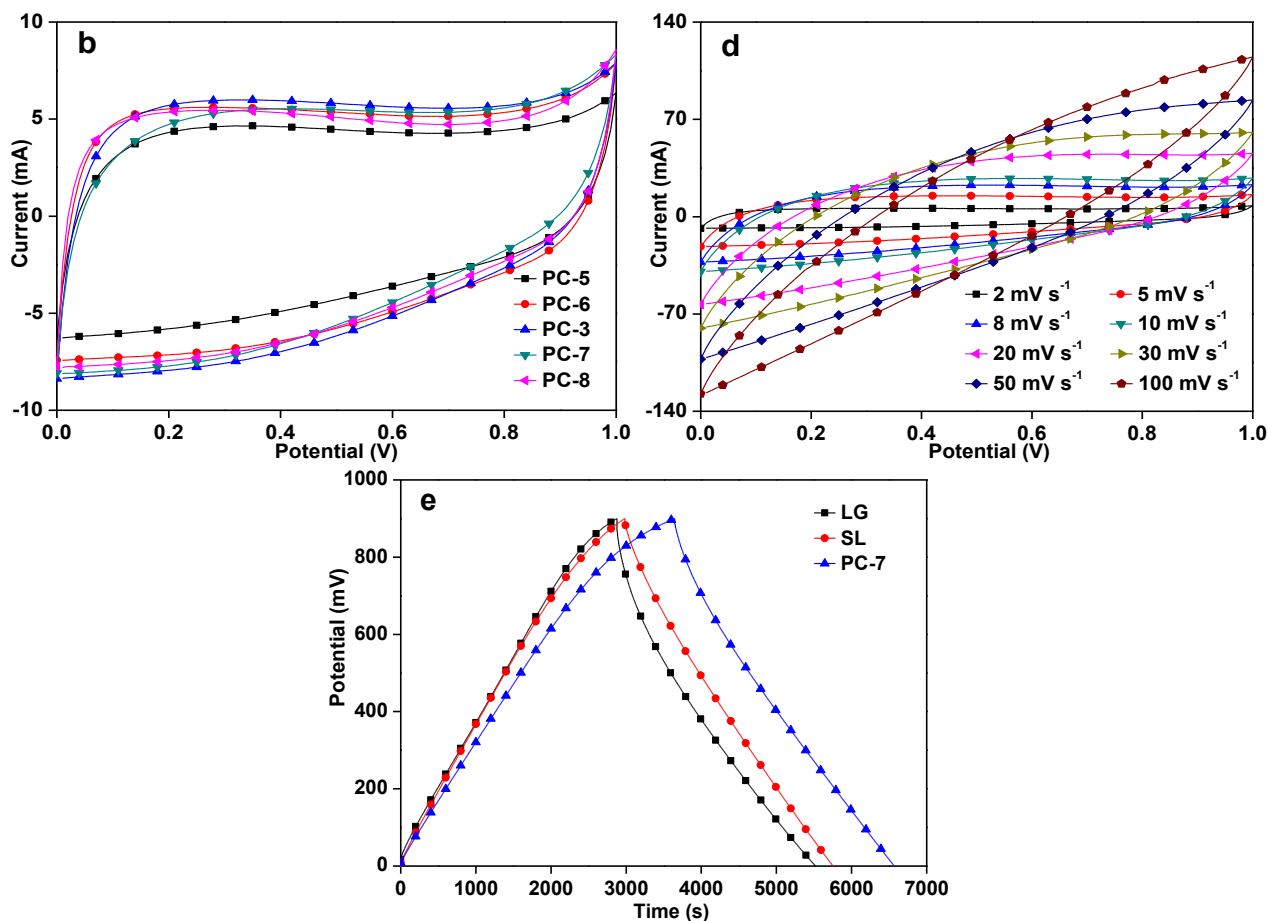


Figure 6. Effect of KOH-LC ratio on the capacitive performances of PCs. GCD curves of PCs with the current density of 40 mA g⁻¹ (a); SSA and C_s at different ratios (b); CV curves at scan rate of 2 mV s⁻¹ (c); PC-3 at various scan rates from 2 mV s⁻¹ to 100 mV s⁻¹ (d); GCD curves of LG, SL and PC-7 (e).

3.2.3. The Effect of Activation Temperatures

In this study, the effects of activation temperature on electrochemical performance of PCs are carried out under the condition that KOH-LC ratio was kept at 3. The GCD curves of PC-9, PC-3, PC-10 and PC-11 are displayed in Fig. 7a. All the GCD curves show an approximate isosceles triangle, indicating good EDLC features and there is no faraday current caused by the redox reactions. In addition, the charge-discharge time of PC-3 is longer than PC-9, PC-10 and PC-11, suggesting the PC-3 has higher C_s under the same current density. As shown in Fig. 7b, the C_s of PC-3 is 280.43 F g⁻¹ at the current density of 40 mA g⁻¹. At the current density of 300 mA g⁻¹, the C_s of PC-3 is retain 227.75 F g⁻¹, which demonstrates that 700 °C is the best activation temperature. The changes are due to the different SSA and pore structures of PCs (Table 3). The CV curves of PC-9, PC-3, PC-10 and PC-11 exhibit the approximate rectangle shapes at 2 mV s⁻¹ in Fig. 7c. The area of the CV curve for the PC-3 is much larger than others, demonstrating the PC-3 has the best electrochemical performances.

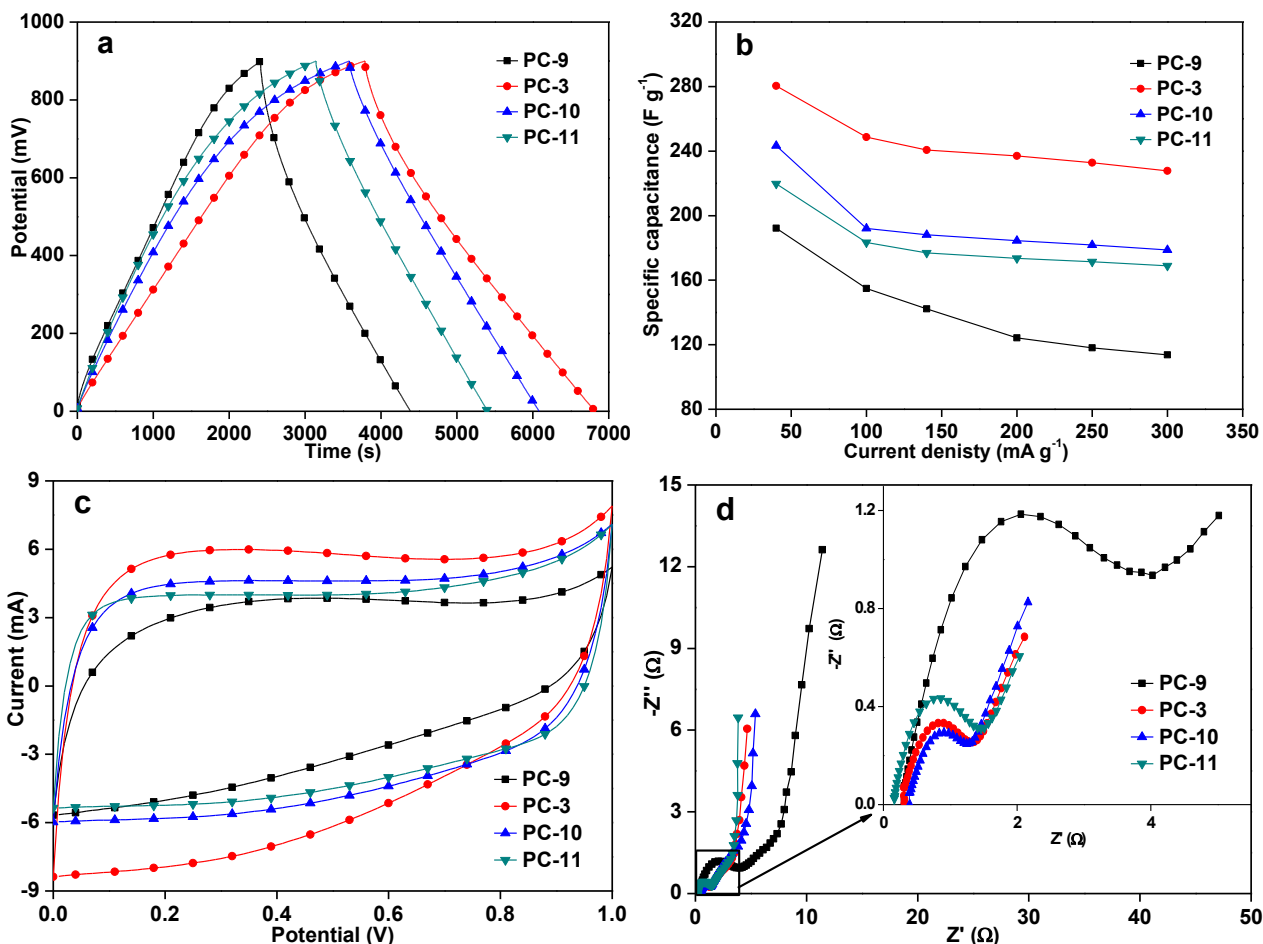


Figure 7. Effects of activation temperatures on the capacitive performances of PCs. GCD curves of PCs at 40 mA g⁻¹ (a); the C_s of PCs under different current densities (b); CV curves of PCs at 2 mV s⁻¹ (c); Nyquist plots of PCs (d).

The EIS test was carried out for further understand the electrochemical behavior and the effect of frequency on the carbon electrodes. As shown in Fig. 7d, all the samples have ideal electrochemical capacitance characteristic. In the low frequency, the Nyquist plots present nearly linear indicating the ideal capacitive behavior [46, 47]. There is a clear semicircle in high frequency, indicating the interface of the electrode exists ion diffusion resistance [48]. The semi-circle of PC-3, PC-10 and PC-11 is smaller than PC-9, indicating the ion diffusion into the electrode surface of PC-3, PC-10 and PC-11 is faster than into PC-9.

The energy density and power density are calculated according to the Eqs. (2) and (3). The plot of PCs with different activation temperatures are shown in Fig. 8. As can be seen, the energy density decreased slowly with the increase of power density, demonstrating that in the high power density less energy was released [49]. The energy density of PC-3 is higher than PC-9, PC-10 and PC-11, indicating the PC-3 possess better electrochemical performances [2, 50]. This is due to the high SSA and larger average pore diameter of PC-3.

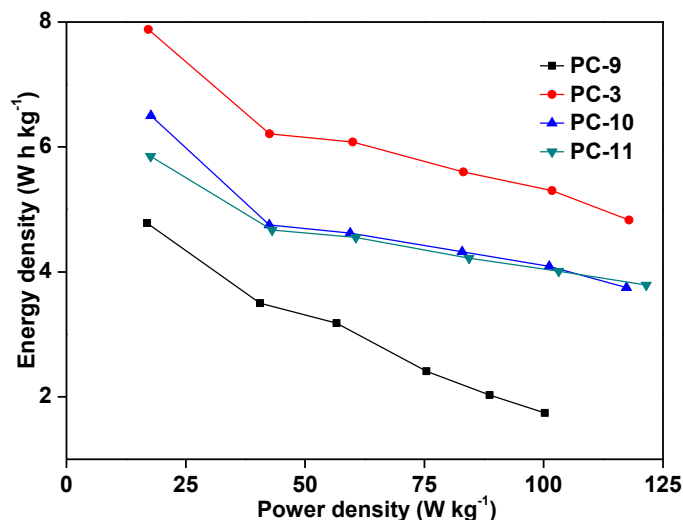


Figure 8. Ragone plot of PCs with different activation temperatures.

To compare the performance of the PCs electrodes, a summary of performance of other PCs electrodes is presented in the Table 4. The PC prepared in this work exhibits large SSA and high C_s , demonstrating that the lignite mixed with lignin chelating with Zn^{2+} derived PCs are highly promising as electrode for EDLC and show excellent electrochemical performance.

Table 4. PCs for EDLC electrodes.

Raw materials	SSA ($m^2 g^{-1}$)	C_s ($F g^{-1}$)	Electrolyte	Ref.
Lignite	1024	207.5 ($500 mA g^{-1}$)	6 M KOH	[33]
HyperCoal	2540	46 ($10 mA g^{-1}$)	0.5 M TEABF ₄ /PC	[14]
Rice husk	2696	147 ($100 mA g^{-1}$)	6 M KOH	[51]
Oil palm kernel shell	462	210 ($500 mA g^{-1}$)	1 M KOH	[52]
Ultra-Pure lignite	1696	189 ($20 mA g^{-1}$)	6 M KOH	[53]
Lignin and lignite	3311	280.43 ($40 mA g^{-1}$)	6 M KOH	This work

4. CONCLUSION

The PCs with high SSA were prepared from lignite mixed with lignin chelating with Zn^{2+} using KOH as activation agent. The Zn^{2+} content, KOH-LC ratio and activation temperature had remarkable influence on the SSA and C_s of PCs. The C_s increased with along with the SSA and the largest SSA reaches to $3311 m^2 g^{-1}$. The addition of lignin chelate with Zn^{2+} to lignite may affect the carbonization-activation process of lignite and improve the performance of PCs. The prepared PCs as electrode materials exhibit excellent electrochemical performance for EDLC. The PC-3 present high C_s of $280.43 F g^{-1}$ at $40 mA g^{-1}$ and the C_s still retain a high value of $227.75 F g^{-1}$ at $300 mA g^{-1}$. Accordingly, the mixture of lignin and lignite has been demonstrated to be a good precursor to prepare the activated carbon and excellent performance electrodes for EDLC.

ACKNOWLEDGEMENTS

This work was subsidized by the Fundamental Research Funds for the Central Universities (China University of Mining & Technology, Grant 2017XKZD10) and the Priority Academic Program Development of Jiangsu Higher Education Institutions.

References

1. X. C. Liu, S. M. Li, R. Mi, J. Mei, L. M. Liu, L. J. Cao, W. M. Lau, H. Liu, *Appl. Energ.*, 153 (2015) 32.
2. M. B. Wu, P. Li, Y. Li, J. Liu, Y. Wang, *RSC Adv.*, 5 (2015) 16575.
3. T. A. Centeno, F. Stoeckli, *Electrochem. Commun.*, 16 (2012) 34.
4. J. Wang, M. M. Chen, C. Y. Wang, J. Z. Wang, J. M. Zheng, *J. Power Sources*, 196 (2011) 550.
5. X. Zhang, L. Y. Ji, S. C. Zhang, W. S. Yang, *J. Power Sources*, 173 (2007) 1017.
6. P. Simon, Y. Gogotsi, *Nature Mater.*, 7 (2008) 845.
7. I. Y. Jang, H. Muramatsu, K. C. Park, Y. J. Kim, M. Endo, *Electrochem. Commun.*, 11 (2009) 719.
8. X. Du, W. Zhao, Y. Wang, C. Wang, M. Y. Chen, T. Qi, C. Hua, M. G. Ma, *Bioresource Technol.*, 149 (2013) 31.
9. T. F. Baumann, M. A. Worsley, T. Y.-J. Han, J. H. Satcher, *J. Non-Cryst. Solids*, 354 (2008) 3513.
10. Z. Q. Hao, J. P. Cao, Y. Wu, X. Y. Zhao, L. Zhou, X. Fan, Y. P. Zhao, X. Y. Wei, *Fuel Process. Technol.*, 162 (2017) 45.
11. X. Y. Zhao, S. S. Huang, J. P. Cao, X. Y. Wei, K. Magarisawa, T. Takarada, *Fuel Process. Technol.*, 125 (2014) 251.
12. C. Peng, X. B. Yan, R. T. Wang, J. W. Lang, Y. J. Ou, Q. J. Xue, *Electrochim. Acta*, 87 (2013) 401.
13. T. E. Rufford, D. Hulicova-Jurcakova, K. Khosla, Z. H. Zhu, G. Q. Lu, *J. Power Sources*, 195 (2010) 912.
14. X. Y. Zhao, S. S. Huang, J. P. Cao, S. C. Xi, X. Y. Wei, J. Kamamoto, T. Takarada, *J. Anal. Appl. Pyrol.*, 105 (2014) 116.
15. M. G. Deng, R. Q. Wang, *New Carbon Mater.*, 28 (2013) 262.
16. X. J. He, R. C. Li, J. S. Qiu, K. Xie, P. H. Ling, M. X. Yu, X. Y. Zhang, M. D. Zheng, *Carbon*, 50 (2012) 4911.
17. J. P. Cao, S. He, Y. Wu, X. Y. Zhao, X. Y. Wei, T. Takarada, *Int. J. Electrochem. Sci.*, 12 (2017) 2704.
18. W. L. Zhang, M. Z. Zhao, R. Y. Liu, X. F. Wang, H. B. Lin, *Colloid. Surf. A: Physicochem. Eng. Asp.*, 484 (2015) 518.
19. D. Saha, Y. C. Li, Z. H. Bi, J. H. Chen, J. K. Keum, D. K. Hensley, H. A. Grappe, H. M. Meyer, S. Dai, M. P. Paranthaman, A. K. Naskar, *Langmuir*, 30 (2014) 900.
20. C. L. Lai, Z. P. Zhou, L. F. Zhang, X. X. Wang, Q. X. Zhou, Y. Zhao, Y. C. Wang, X. F. Wu, Z. T. Zhu, H. Fong, *J. Power Sources*, 247 (2014) 134.
21. S. Hong, H. L. Lian, X. Sun, D. Pan, A. Carranza, J. A. Pojman, J. D. Mota-Morales, *RSC Adv.*, 6 (2016) 89599.
22. L. N. Liu, G. B. Huang, P. G. Song, Y. M. Yu, S. Y. Fu, *ACS Sustain. Chem. Eng.*, 4 (2016) 4732.
23. C. H. Lei, N. Amini, F. Markoulidis, P. Wilson, S. Tennison, C. Lekakou, *J. Mater. Chem. A*, 1 (2013) 6037.
24. X. J. He, P. H. Ling, M. X. Yu, X. T. Wang, X. Y. Zhang, M. D. Zheng, *Electrochim. Acta*, 105 (2013) 635.
25. X. J. He, Y. J. Geng, J. S. Qiu, M. D. Zheng, S. Long, X. Y. Zhang, *Carbon*, 48 (2010) 1662.
26. J. B. Zhang, L. J. Jin, J. Cheng, H. Q. Hu, *Carbon*, 55 (2013) 221.
27. R. Farma, M. Deraman, A. Awitdrus, I. A. Talib, E. Taer, N. H. Basri, J. G. Manjunatha, M. M. Ishak, B. N. Dollah, S. A. Hashmi, *Bioresource Technol.*, 132 (2013) 254.

28. X. X. Xiang, E. H. Liu, Z. Z. Huang, H. J. Shen, Y. Y. Tian, C. Y. Xiao, J. J. Yang, Z. H. Mao, *J. Solid State Electr.*, 15 (2010) 2667.
29. Ö. Şahin, C. Saka, A. A. Ceyhan, O. Baytar, *Sep. Sci. Technol.*, 50 (2014) 886.
30. S. Yorgun, N. Vural, H. Demiral, *Micropor. Mesopor. Mater.*, 122 (2009) 189.
31. D. C. Liu, W. L. Zhang, H. B. Lin, Y. Li, H. Y. Lu, Y. Wang, *J. Clean. Prod.*, 112 (2016) 1190.
32. X. L. Song, Y. Zhang, C. M. Chang, *Ind. Eng. Chem. Res.*, 51 (2012) 15075.
33. L. J. Li, X. Y. Wang, S. J. Wang, Z. Z. Cao, Z. J. Wu, H. Wang, Y. F. Gao, J. R. Liu, *Electroanaly.*, 28 (2016) 243.
34. C. F. Chang, C. Y. Chang, W. T. Tsai, *J. Colloid Interf. Sci.*, 232 (2000) 45.
35. J. Matos, M. Labady, A. Albornoz, J. Laine, J. L. Brito, *J. Mol. Catal. A: Chem.*, 228 (2005) 189.
36. J. Chmiola, G. Yushin, R. Dash, Y. Gogotsi, *J. Power Sources*, 158 (2006) 765.
37. E. Raymundo-Piñero, K. Kierzek, J. Machnikowski, F. Béguin, *Carbon*, 44 (2006) 2498.
38. J. Sheng, C. Ma, Y. Ma, H. X. Zhang, R. R. Wang, Z. Y. Xie, J. L. Shi, *Int. J. Hydrogen Energy*, 41 (2016) 9383.
39. S. H. Du, L. Q. Wang, X. T. Fu, M. M. Chen, C. Y. Wang, *Bioresource Technol.*, 139 (2013) 406.
40. X. L. Gao, W. Xing, J. Zhou, G. Q. Wang, S. P. Zhuo, Z. Liu, Q. Z. Xue, Z. F. Yan, *Electrochim. Acta*, 133 (2014) 459.
41. W. Xing, S. Z. Qiao, R. G. Ding, F. Li, G. Q. Lu, Z. F. Yan, H. M. Cheng, *Carbon*, 44 (2006) 216.
42. M. Biswal, A. Banerjee, M. Deo, S. Ogale, *Energ. Environ. Sci.*, 6 (2013) 1249.
43. J. Gamby, P. L. Taberna, P. Simon, J. F. Fauvarque, M. Chesneau, *J. Power sources*, 101 (2001) 109.
44. V. Subramanian, C. Luo, A. M. Stephan, K. S. Nahm, S. Thomas, B. Q. Wei, *J. Phys. Chem. C*, 111 (2007) 7527.
45. B. B. Chang, Y. L. Wang, K. M. Pei, S. M. Yang, X. P. Dong, *RSC Adv.*, 4 (2014) 40546.
46. Y. Fan, X. Yang, B. Zhu, P. F. Liu, H. T. Lu, *J. Power Sources*, 268 (2014) 584.
47. Y. Gao, L. Li, Y. M. Jin, Y. Wang, C. J. Yuan, Y. J. Wei, G. Chen, J. J. Ge, H. Y. Lu, *Appl. Energ.*, 153 (2015) 41.
48. M. Sevilla, W. Gu, C. Falco, M. M. Titirici, A. B. Fuertes, G. Yushin, *J. Power Sources*, 267 (2014) 26.
49. X. Li, W. Xing, S. P. Zhuo, J. Zhou, F. Li, S. Z. Qiao, G. Q. Lu, *Bioresource Technol.*, 102 (2011) 1118.
50. A. Jain, C. H. Xu, S. Jayaraman, R. Balasubramanian, J. Y. Lee, M. P. Srinivasan, *Micropor. Mesopor. Mater.*, 218 (2015) 55.
51. E. Y. L. Teo, L. Muniandy, E.-P. Ng, F. Adam, A. R. Mohamed, R. Jose, K. F. Chong, *Electrochim. Acta*, 192 (2016) 110.
52. I. I. Misnon, N. K. M. Zain, R. A. Aziz, B. Vidyadharan, R. Jose, *Electrochim. Acta*, 174 (2015) 78.
53. M. Y. Zhang, X. Zhao, Q. C. Zhuang, *Int. J. Electrochem. Sci.*, 11 (2016) 2153.